Journal of Materials Chemistry A

Accepted Manuscript

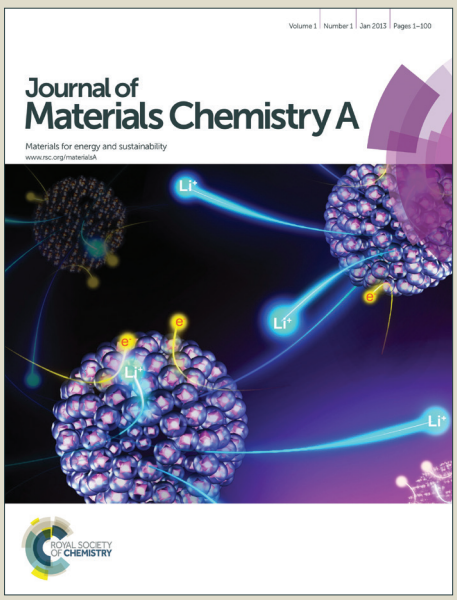

This is an *Accepted Manuscript*, which has been through the Royal Society of Chemistry peer review process and has been accepted for publication.

Accepted Manuscripts are published online shortly after acceptance, before technical editing, formatting and proof reading. Using this free service, authors can make their results available to the community, in citable form, before we publish the edited article. We will replace this *Accepted Manuscript* with the edited and formatted *Advance Article* as soon as it is available.

You can find more information about *Accepted Manuscripts* in the Information for Authors.

Please note that technical editing may introduce minor changes to the text and/or graphics, which may alter content. The journal's standard Terms & Conditions and the Ethical guidelines still apply. In no event shall the Royal Society of Chemistry be held responsible for any errors or omissions in this *Accepted Manuscript* or any consequences arising from the use of any information it contains.

ROYAL SOCIETY OF CHEMISTRY

www.rsc.org/materialsA

Journal of
Materials Chemistry A

RSCPublishing

Paper

A channel-type mesoporous In(III)–carboxylate coordination framework with high physicochemical stability for electrode material of supercapacitor

Cite this: DOI: 10.1039/xoxxoooooox

Received ooth January 2014,
Accepted ooth January 2014

DOI: 10.1039/xoxxoooooox

www.rsc.org/MaterialsA

Miao Du,*[a] Min Chen,[b] Xiao-Gang Yang,[b] Jiong Wen,[b] Xi Wang,[a] Shao-Ming Fang[b] and Chun-Sen Liu*[b]

Stability is the most critical problem which will hinder the practical applications of metal–organic frameworks (MOFs), which are normally destroyed upon heating or facing chemicals to reduce or even lose their porous nature. Herein, we present a mesoporous 437-MOF material with perfect 1-D hexagonal channels of ca. 3 nm pore size, which shows high thermal and chemical stability. The gas sorption capability of desolvated 437-MOF can be improved by activating the material at higher temperatures. Remarkably, the optimal porosity will be achieved by using a combined approach via treating the sample in boiling water and further heating. This unexpected observation can be ascribed to the synergy effects of external and internal surfaces of the porous crystalline material. Exploration of its possible applications in supercapacitor shows a great potential of activated 437-MOF as the electrode material, in virtue of its higher surface area (ca. 2400 $m^2 g^{-1}$), hierarchical pore structures, and the contribution of pseudocapacitor provided by In-doping.

Introduction

Metal–organic frameworks (MOFs) represent a burgeoning type of porous crystalline materials with permanent porosity, higher surface areas, tunable pore sizes, and a wide range of possible applications,[1] which can be considered as the bridge between traditional zeolites and mesoporous silica.[2,3] Thus far, abundant MOFs with micropores (pore size < 2 nm) have been reported, while mesoporous MOFs (mesoMOFs, 2 nm < pore size < 50 nm) are extremely unusual (Table S1 and Table S2). However, the applications of microporous MOFs will be largely restricted because their narrower pores cannot accommodate larger guest components and anchor molecular functions, which will also hinder fast molecular diffusion and mass transfer.[4a] In comparison, mesoMOFs materials can meet such requirements, which thus not only make great success in the application domains of microporous MOFs and traditional mesoporous materials, but also have significant superiority over them.[4b,4c] In fact, the design and preparation of mesoMOFs are quite difficult, because the coordination frameworks are apt to interpenetrate or even collapse when the pores are expanded.[5] Further, the large pores that are mainly sustained by flexible coordination bonding also usually result in their poor physicochemical stability upon external stimuli such as heating or water, which represents one of the most great challenges at this stage.[6]

Currently, most MOFs are constructed by divalent metal cations (e.g. Zn^{2+} and Cu^{2+})[1] and those based on trivalent metals (such as Al^{3+}, Cr^{3+}, or In^{3+}) are relatively rare,[7,8] which however can improve the chemical stability (for example, towards hydrolysis) of the resulting coordination frameworks.[2a,8] In this connection, In(III) will be a promising candidate for constructing MOFs for its low toxicity and high water stability.[9] On the other hand, ligand extension strategy is quite effective to design MOFs with large pores, as confirmed by the success in designing and preparing two isoreticular series of MOF-5 and MOF-74 porous materials.[10,11] Also, the extended trigonal tectons (see Scheme S1) based on trimesic acid have been extensively applied to construct diverse MOFs, which can be finely regulated by changing the sizes and steric effect of such organic building blocks.[12] In this work, we select 4,4',4''-(benzene-1,3,5-triyl-tris(oxy))tribenzoic acid (H_3BTTB) as the ligand due to its rigid backbone and flexible linkage of the ether oxygen groups. As a result, a new type of In(III) mesoMOF material with uniform 1-D hexagonal channels can be obtained, which has high thermal and chemical stability. Moreover, it should be noted that a crystallographically mesoscale pore does not often represent a real permanent mesopore observed in practice.[4b] Herein, this issue can be well solved by developing a unique combined approach to activate the mesoMOF material in boiling water plus heating. The results can be properly explained by considering the morphology of crystalline material. Notably, this activated mesoMOF is a promising candidate as electrode material for making high-performance supercapacitor that can be retained after cycling at least 6000 times.

Journal of Materials Chemistry A Accepted Manuscript

Experimental

Synthesis of $\{[In(BTTB)_{2/3}(OH)](NMF)_5(H_2O)_4\}_n$ (437-MOF)

A mixture including $In(NO_3)_3$ (3.61 g, 12 mmol), H_3BTTB ligand (2.92 g, 6 mmol), and *N*-methylformamide (NMF) (30 mL) was stirred in a vial (50 mL) for 2 hours at room temperature. Then, the vial was sealed into a Teflon-lined stainless steel vessel, which was heated at 120 °C for 5 days in an oven. After cooling to room temperature, colorless crystal products for 437-MOF were obtained in ca. 70% yield (2.3 g, based on H_3BTTB). Notably, most products were collected as the microcrystalline grains and only several pieces of single crystals can be selected for X-ray diffraction. Elemental analysis (percentage calculated / experimental) for $C_{28}H_{44}O_{16}InN_5$: C, 40.94 / 40.69; H, 5.40 / 5.23; and N: 8.53 / 8.50. FT-IR (cm^{-1}): 3415vs (br), 1618s, 1596vs, 1560w, 1541w, 1535w, 1501w, 1458w, 1406vs, 1228s, 1164m, 1185w, 1009w, 854w, 785w, 618m, 472w.

Activation of 437-MOF-80, 437-MOF-240, and 437-MOF-360

The as-synthesized 437-MOF sample (ca. 80 mg) was soaked in CH_2Cl_2 (20 mL) for 1 day, and the extract was discarded. Fresh CH_2Cl_2 was subsequently added, and the sample was allowed to soak for another 24 hours to eliminate any NMF and H_2O. Such a refilling and removing recycle was repeated three times. After removal of CH_2Cl_2 by decanting, the sample was transferred to a pre-weighed 12-mm sample tube, evacuated (< 10^{-3} Torr) at room temperature overnight, then dried again using the 'outgas' function of the adsorption instrument for 10 hours at 80 °C (for 437-MOF-80), 6 hours at 240 °C (for 437-MOF-240), and 6 hours at 360 °C (for 437-MOF-360), respectively, prior to gas adsorption/desorption measurements.

Activation of 437-MOF-boiling water and 437-MOF-boiling water-3h

The as-synthesized 437-MOF sample (ca. 80 mg) was dispersed into water (30 mL) in a vial, sealed into a Teflon-lined stainless steel vessel, and then heated at 100 °C in an oven for 1 hour (437-MOF-boiling water) or 3 hours (437-MOF-boiling water-3h). The resulting solid was cooled down and filtered. Then, the sample was soaked in CH_2Cl_2 for 24 hours, and the extract was discarded. Fresh CH_2Cl_2 was subsequently added, and the sample was allowed to soak for 24 hours to eliminate any NMF and H_2O. Such a refilling and removing recycle was repeated three times. After CH_2Cl_2 was removed by decanting, the sample was transferred to a pre-weighed 12-mm sample tube, evacuated (< 10^{-3} Torr) at room temperature overnight, then dried again by using the 'outgas' function of the adsorption instrument for 10 hours at 120 ºC prior to adsorption/desorption measurements.

Electrochemical tests

Electrochemical tests of individual electrode were performed in a three-electrode system with KOH (6 mol L^{-1}) electrolyte. The activated material 437-MOF on nickel mesh, a platinum rod, and a saturated calomel electrode (SCE) were used as the working, counter, and reference electrode, respectively. The working electrode is composed of activated 437-MOF (80 wt%), conductive material (acetylene black, ATB, 10 wt%), and binder (polytetrafluoroethylene, PTFE, 10 wt%). The mixture was first coated onto the surface of a piece of nickel foam sheet (1 × 1 cm^2), dried at 100 °C for 12 hours, and finally pressed under 10 MPa to give the working electrode. Cyclic voltammogram (CV) curves were recorded with a CHI 660D electrochemical workstation. Galvanostatic charge/discharge cycles were measured on a CT2001A LAND Cell test system. Electrochemical impedance spectroscopy (EIS) measurements were taken on a CHI 660D electrochemical workstation by applying an AC signal of 0.2 V. Herein, all electrochemical tests were carried out at room temperature.

Results and discussion

Crystal structure and topological analysis

Solvothermal reaction of H_3BTTB with $In(NO_3)_3$ produces the solvated complex $\{[In(BTTB)_{2/3}(OH)](NMF)_5(H_2O)_4\}_n$ (437-MOF) in gram-scale with high yield. 437-MOF (space group $P6_3/mcm$) has a 3-D mesoporous coordination framework with regular 1-D hexagonal channels. The asymmetric coordination unit consists of one In(III) ion with 1/4 occupancy, 1/6 BTTB ligand, and one hydroxyl with 1/4 occupancy (see Fig. S2). The octahedral In(III) center is surrounded by four carboxylates and two μ-OH^- anions (Fig. S3), in which the BTTB ligand is fully deprotonated to link six In(III) centers (Fig. S4). Two adjacent InO_6 octahedra share the axial μ-OH^- to construct an unusual $[In(OH)]_n$ rod-shaped inorganic chain (Fig. S5) as the secondary building units (SBUs). The intrinsic packing arrangement of such SBUs will effectively prevent the network interpenetration and further augment the channel sizes of MOFs.[13] Notably, this strategy mostly succeeds in the design of microporous MOFs, instead of their mesoporous analogues.[13,14] For known In(III)–carboxylate coordination frameworks, the $[In(O_2CR)_4]$ monomer and $[In_3O(O_2CR)_6(H_2O)_3]$ trimer are very common, whereas $[In(OH)]_n$ SBU is scarcely observed.[7a]

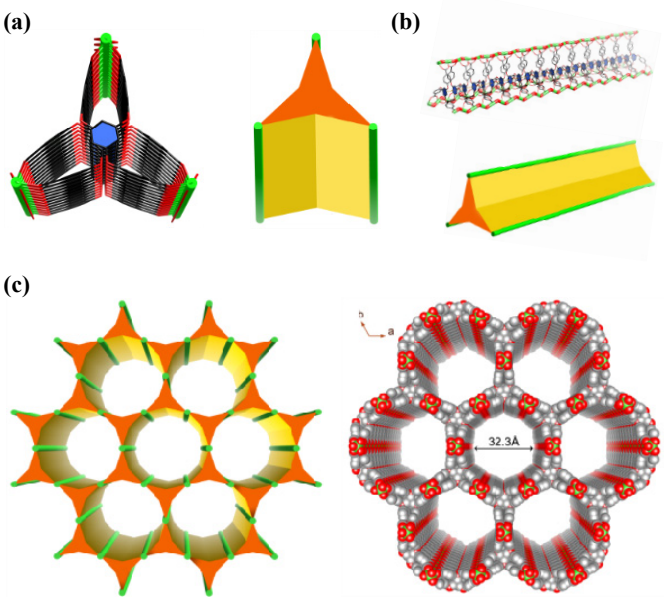

Fig. 1 Crystal structure of 437-MOF. (a) Top and schematic views of the concave triangular prism SBB. (b) Side and schematic views of the concave triangular prism SBB. (c) View of the 3-D framework and the space-filling model showing regular 1-D hexagonal channels.

The flexible BTTB ligand has a unique conformation of high symmetry (Fig. S6 and Fig. S7), where three benzene arms and the attached carboxylates are perpendicular to the benzene core, and the center of benzene core is located at the centroid of the equilateral triangle comprising three carboxylate carbon atoms. This unique conformation has not been observed in all known MOFs with such extended trigonal ligands (Table S5). Obvious

Journal of Materials Chemistry A Accepted Manuscript

This journal is © The Royal Society of Chemistry 2014

π···π stacking interactions occur between the parallel benzene cores of BTTB ligands (centroid-to-centroid distance: 3.635 Å) to produce a 1-D organic supramolecular array along the *c* axis (Fig. S8 and Fig. S9). The combination of such organic arrays and rod-shaped inorganic SBUs affords a 1-D concave triangular prism that acts as a supermolecular building block (SBB,[15] an extension of SBU, see Fig. 1a and Fig. 1b). Notably, infinite SBB is unknown in MOFs chemistry, although various discrete SBUs or SBBs and infinite SBUs have been reported thus far. Such large and robust SBBs share the inorganic SBUs to form a 3-D coordination network (see Fig. 1c), which will enlarge its channel size and also enhance the structural stability, from the viewpoint of architecture engineering design.

The 3-D framework of 437-MOF consists of uniform hexagonal mesoporous channels of 32.3 Å (measured between In(III) atoms on opposite pore walls) or 28.4 Å (considering van der Waals radii of atoms) along the *c* axis, with the calculated free volume by PLATON[16] of 4292.4 Å^3 (65.3%, 1.8 Å probe radius). Analysis of the known mesoMOFs (Table S1) reveals that the cage-type mesoMOFs (mesoporous cavities surrounded by microporous windows) are mostly common (53.5%) and those of 3-D channel-type are also familiar (32.4%). In contrast, mesoMOFs with uniform 1-D channels are quite scarce, where only JUC-48[17] and an isoreticular series of MOF-74[11] materials have been known, in addition to CYCU-3 with both microporous and mesoporous channels.[18] In fact, 437-MOF represents the first mesoMOF with uniform 1-D hexagonal channels owing to its higher 6-fold symmetry.

Herein, the connectivity of triangular prism nodes for BTTB ligands and hexagonal nodes for In(III) ions results in a 2-nodal 6-connected 3-D $(3^3.4^6.5^6)_2(3^4.4^4.5^4.6^3)_3$ net (Fig. S10), which is unknown although 6-connected networks are quite familiar in MOFs.[19] Alternatively, this structure can also be considered as a (3,4)-connected $(4^2.6^3.8)_3(6^3)$ topological network constructed by 1-D In–O SBUs and 3-connected BTTB ligands (Fig. S11). Notably, the hexagonal channel arrays for 437-MOF seem similar to carbon nanotubes with the hybridized 1-D In–O inorganic moiety (Fig. S12), in which the impenetrable aromatic walls of the tubular channels can readily avoid the network interpenetration to afford the resulting mesoporous framework.

Physicochemical stability and porosity

The main defect of MOFs is their poor stability, especially for mesoMOFs, which will directly hinder their applications. Normally, most MOFs materials will suffer in thermal stability, when the pores are extended from microporous to mesoporous region.[4] Thermogravimetric analysis curve of 437-MOF reveals that the framework can keep stable to 400 °C (Fig. S1), which can even tolerate the prolonged heating in vacuum (see Thermal stability in ESI†). Another trouble of MOFs materials is their lower chemical stability, and in this point, water stability will be always vital for its ubiquitous nature. However, instability in water phase is usually observed for most MOFs, mainly caused by metal hydrolysis.[20] Notably, 437-MOF remains highly stable in cool water for weeks or even in boiling water in a short period. In addition, the structural resistance of 437-MOF against common organic solvents and acid or base solution can also be confirmed (see Chemical stability in ESI†). The unusual physicochemical stability (Fig. 2) of 437-MOF should be closely related to its structural features, which may facilitate the potential functional applications. Herein, some slight differences in peak intensity of powder X-ray diffraction (PXRD) patterns can be properly attributed to the preferred orientation of microcrystalline samples.

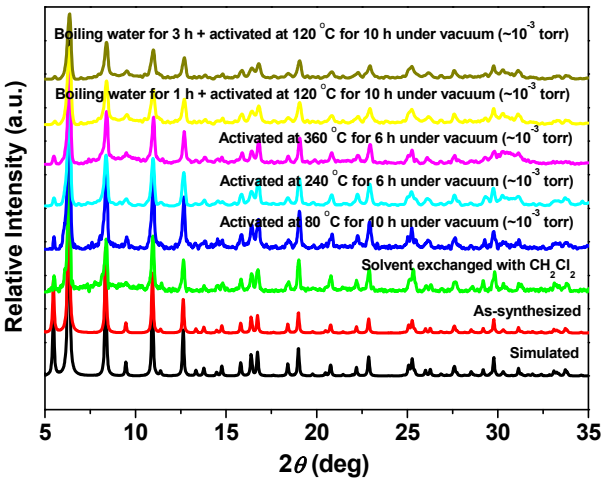

Fig. 2 Powder X-ray diffraction (PXRD) patterns of 437-MOF samples.

Considering the large 1-D channels and high physicochemical stability, the porosity of 437-MOF was evaluated by gas adsorption. The CH_2Cl_2-exchanged 437-MOF sample was activated at 80 °C to afford the desolvated material 437-MOF-80, and the N_2 sorption result reveals that the framework is highly porous and displays an isotherm of mesoporosity (see Fig. 3a). The Brunauer-Emmett-Teller (BET) surface area of 1576 m^2 g^{-1} can be calculated from the first plateau in isotherm for surface adsorption within the channels,[21] and the second steep rise with $P/P_0 \sim 0.2$ reveals the filling of N_2 in mesopores. Similar sorption behaviors have also been found in the typical mesoMOFs materials.[6,11] The maximum pore volume (0.92 cm^3 g^{-1}) upon saturation (ca. 600 cm^3 g^{-1}) is consistent with the theoretical value (0.95 cm^3 g^{-1}) calculated from crystal structure. The pore size distribution derived from the N_2 sorption isotherm (Fig. 3b) also agrees well with the structural analysis. Normally, higher activated temperature will promote the adsorption capacities of MOFs.[22] For the sample activated at 240 °C (437-MOF-240), the N_2 isotherm shows a similar adsorption behavior (see Fig. 3a). However, the N_2 uptake, BET surface area, and maximum pore volume are all increased (see Table S6). This result can be ascribed to a trace amount of solvents resided in the 1-D channels of 437-MOF-80 with an insufficient activation at 80 °C (Fig. S18).[23] Of further significance, a symptom of hysteresis loop can be observed in this case, which is associated with the capillary condensation occurring in the mesopores.[24] When the activated temperature is raised to 360 °C, the N_2 isotherm of 437-MOF-360 shows the typical hysteresis loop of mesoporous materials,[24] although the maximum uptake is reduced (see Fig. 3a). In comparison with that of 437-MOF-240, the lower surface area of 437-MOF-360 sample (Table S6) may indicate the partial damage of material, which contains a trace amount of In_2O_3 as recognized from its PXRD pattern (Fig. S13).

In this context, it can be concluded that increasing the activated temperature will facilitate higher gas uptake but can also be harmful to keep the integrality of MOFs materials. Thus, to achieve the optimal porosity, the development of new activated method will be significant. Here, 437-MOF shows considerable chemical stability toward boiling water, and the channel walls will be hydrophobic according to its crystal structure, which is also confirmed by vapor adsorption analysis (see ESI† for details). Thus, the 437-MOF sample was activated in boiling water with subsequent heating. Remarkably, the activated sample 437-MOF-boiling water displays a clear change in N_2 isotherm

Journal of Materials Chemistry A Accepted Manuscript

(see Fig. 3a). The typical hysteresis loop definitely reveals the mesoporous nature of 437-MOF-boiling water, which significantly exhibits the optimal porosity for N_2 uptake (723 cm^3 g^{-1}), BET surface area (2379 m^2 g^{-1}), and pore volume (1.11 cm^3 g^{-1}), in comparison with those of other samples. However, if 437-MOF was treated in boiling water for 3 h, a significant decrease of N_2 isotherm is observed (Fig. 3a). Notably, this adsorption isotherm shows a very sharp increase near the saturation pressure region (P/P_0 ~ 0.9−1.0), which can be properly attributed to sorption in coarse mesopores and macropores of the materials (textural porosity).[24]

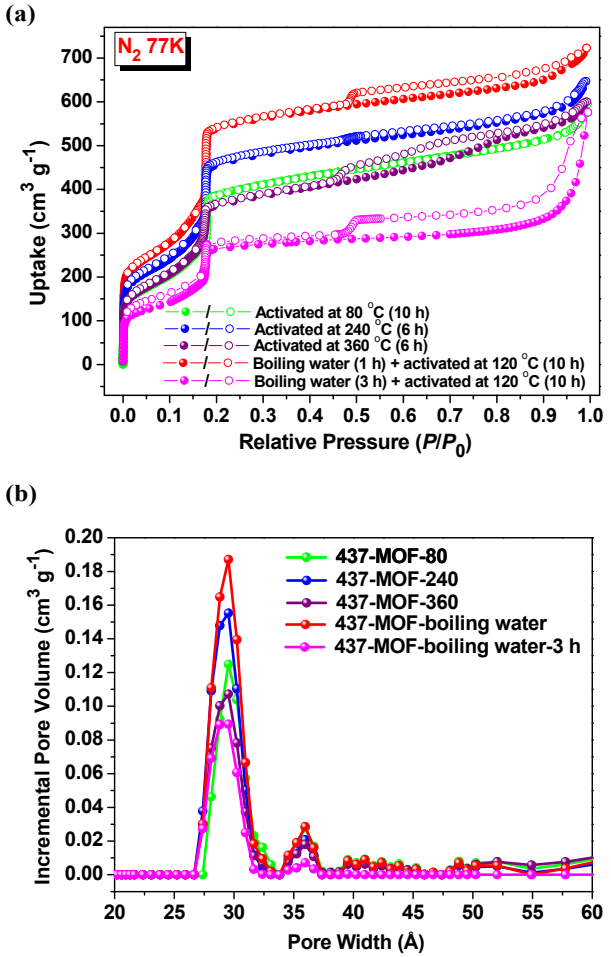

Fig. 3 (a) N_2 sorption isotherms at 77 K for 437-MOFs activated at different conditions (filled/open circles: adsorption/desorption). (b) Pore size distribution plots of 437-MOF-80, 437-MOF-240, 437-MOF-360, 437-MOF-boiling water, and 437-MOF-boiling water-3h.

For water stability which is important for any sorbent to be used practically,[2a,20] almost all MOFs with water stability have only been validated by PXRD patterns. In fact, gas sorption will provide the most convictive evidence for permanent porosity of MOFs, while PXRD can only partially support their framework stability. In this regard, water stability of PCN-222 and MIL-101 has been testified by N_2 sorption isotherms, which are almost unchanged after treating with boiling water.[6,8] While for 437-MOF-boiling water sample, the hysteresis loop for mesopore is more clear, its N_2 uptake and surface area increase, and moreover, the pore volume exceeds the calculated value. Fortunately, a careful screening of 437-MOF-boiling water crystals (before heating in vacuum) allows us to further carry out the single crystal X-ray diffraction. The result shows that the structure is intact after this treatment, which thus, excludes the possible structural expansion (Table S3). This powerful crystallographic evidence seems to be in conflict with its overflow pore volume after full activation. To clarify the source of additional porosity, we attempt to find some clues from the morphological view. Scanning electron microscopy (SEM) images of freshly synthesized 437-MOF reveal its hexagonal prism morphology in micrometer range, which is a representation of its crystallographic symmetry. As expected, the crystalline sample is very smooth in both surface and interior (Fig. 4a−4c). The SEM images of 437-MOF-boiling water clearly demonstrate the substantial perturbation of crystal surface with the ordered channel-like morphology (see Fig. 4d−4f), which should result from the attack of water molecules. Such channel-like grooves in surface could be defined as the internal surface of porous solids, which is composed of the walls of all cracks, pores, and cavities that are deeper than they are wide,[24] and thus contributes to the excessive gas uptake and pore volume. The SEM images of 437-MOF-boiling water-3h crystal shows a highly porous morphology with honeycomb macropores (Fig. 4g−4i), which can also support its N_2 sorption isotherm.

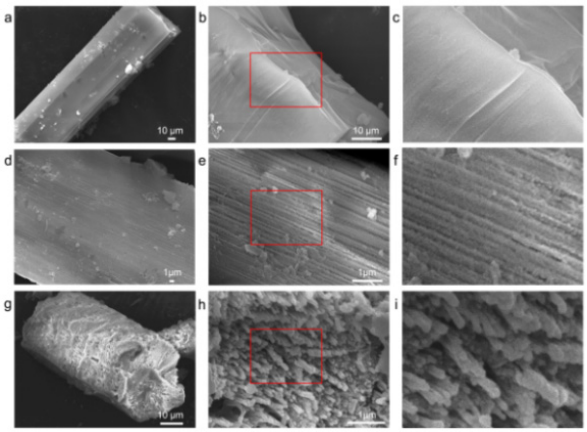

Fig. 4 SEM images of (a) and (b) as-synthesized 437-MOF and (c) the same sample at higher magnification of the red pane; (d) and (e) 437-MOF-boiling water and (f) the same sample at higher magnification of the red pane; (g) and (h) 437-MOF-boiling water-3h and (i) the same sample at higher magnification of the red pane.

The permanent porosity of 437-MOFs was also confirmed by Ar, O_2, and CO_2 adsorption, and all samples keep good crystallinity after gas sorption (see Fig. S19−S23). In each case, the adsorption tendency for Ar or O_2 is comparable to that of N_2 (Fig. S24 and Fig. S25). However, the CO_2 sorption isotherms show two inflection and pronounced steps and then reach saturation, which arise from the electrostatic interactions between CO_2 molecules.[25] The desorption isotherms also show two steps accordingly, but for that of 437-MOF-boiling water, it does not trace the sorption process, which reveals that the adsorbed CO_2 will not be immediately released by reducing the pressure (Fig. S26). In brief, the sorption quantity for all gases will increase in the sequence of 437-MOF-80 ~ 437-MOF-360 < 437-MOF-240 < 437-MOF-boiling water (Table S7). Notably, the surface area of 437-MOF-boiling water is highest among all reported In(III)-based MOFs,[26] and its maximum storages for Ar, O_2, and CO_2 also renew the records of such materials (Table S8).

Journal of Materials Chemistry A Accepted Manuscript

This journal is © The Royal Society of Chemistry 2014

Application of electrode material for supercapacitor

The above results undoubtedly show that 437-MOF with broad gas adsorption capacity may act as a promising mesoMOF material, in the light of its high physicochemical stability. Moreover, the crystal structure of 437-MOF also reveals its similarity to carbon nanotubes, which have been widely used as electrode materials for supercapacitor.[27a] Thus, considering the large surface area, high stability, and nice corrosion resistance of 437-MOF which are essential for electrode material of supercapacitor,[27b] a supercapacitor with 437-MOF-boiling water as electrode material was made. The galvanostatic discharge curves of 437-MOF electrode (Fig. 5a) show the potential windows from –0.7 to 0.3 V. The specific capacitances calculated from the equation $C(F/g) = i\Delta t / m\Delta V$[28] are 150.2, 92, 81, 72, 64, and 56 F g^{-1} at a current density of 0.2, 0.5, 1, 2, 4, and 8 A g^{-1}. The specific capacitance of 437-MOF electrode should benefit from its higher surface area, the hierarchical pore structure that will facilitate the free entry/exit of hydroxyl, and the pseudocapacitance provided by the redox reaction of In(III), which will jointly contribute to the substantial level of capacitive ability.

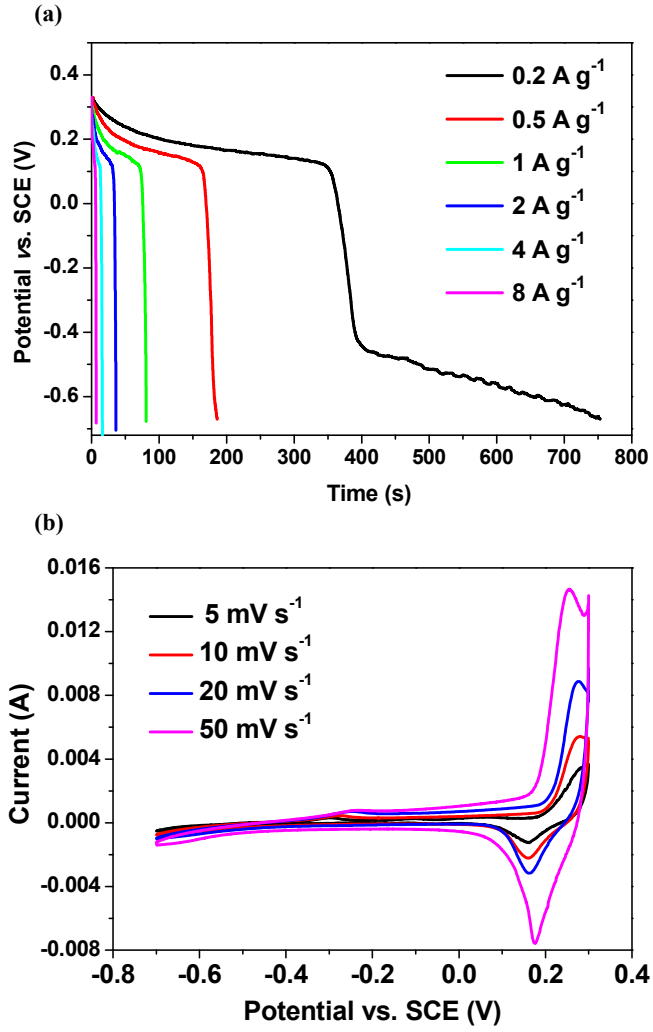

Fig. 5 (a) Galvanostatic discharge curves of 437-MOF electrode at different current densities. (b) CV curves of 437-MOF electrode with different scan rates.

Cyclic voltammogram (CV) curves were recorded to further identify the charge storage mechanism of 437-MOF electrode. As shown in Fig. 5b, a pair of well-defined redox peaks is observed in the CV curve, confirming that the pseudocapacitance originates from the Faradic redox reaction of In(III) ions.[29] Also, the CV curves of 437-MOF electrode with different scan rates reveal that its electrochemical capacitance should mainly result from the pseudocapacitance. The average specific capacitances are calculated to be 98.3, 83.1, 62.1, and 55.5 F g^{-1} at the scan rates of 5, 10, 20, and 50 mV s^{-1}.[28a] The decrease of capacitances along with the increase of scan rates may result from the circuitous diffusion of electrolyte ions into the pores of 437-MOF and the electrode resistance.[30] Similar to most of pseudocapacitance materials, the positive sweeps of CV curves of 437-MOF are not symmetric to their corresponding negative sweeps, which may be caused by polarization and ohmic resistance during the Faradaic process.[31]

For practical applications of supercapacitors, the long term cycle ability is also critical. The galvanostatic charge/discharge curve (Fig. 6a inset) shows that the charge/discharge process of 437-MOF electrode is highly reversible. Moreover, the cycling performance (see Fig. 6a) test indicates that the capacitance of this device will keep unchanged and maintain ca. 100% of its maximum value after cycling 6000 times, revealing the stability of this electrode.[28a,28c,32] The results suggest that 437-MOF may act as a promising candidate for high-performance supercapacitor. However, it must be noted that though the specific capacitance of 437-MOF electrode far exceeds those of carbon-based materials, it may suffer from the relatively lower conductivity, as that observed in transition metal oxides and conducting polymers.[33] To improve their electric conductivity, the composites have been developed in which the metal oxide and conducting polymers can be combined with the highly conductive materials such as carbon or metal nanoparticles.[28a,28c,34] Further, the electrochemical impedance spectroscopy (EIS) is used to evaluate the kinetic and mechanistic information of 437-MOF electrode. Fig. 6b shows a typical Nyquist plot for high conductivity electrode,[35a] in which only a straight line at lower frequency region is observed, showing a Warburg impedance related to the diffusion of electrolyte within the pores of electrode. No semicircle was found in the high-frequency region at the operating voltage of 0.2 V, which can be attributed to the minor effect of interfacial impedance.[35b] The real-axis intercepted at higher frequency corresponds to the uncompensated resistance of electrolyte solution, also known as equivalent series resistance (ESR). The magnitude of ESR gained from the x-intercept of impedance spectra for 437-MOF is 0.4 Ω, which is relatively lower.[36] The curve at lower frequency has a higher angle than 45°, revealing that the electrochemical capacitive behavior is not controlled by diffusion process for 437-MOF electrode, which can facilitate ionic motion in solid electrode.

Conclusions

In summary, a unique mesoporous 437-MOF material has been designed and constructed, which possesses one of the largest 1-D regular channels, permanent mesoporosity, and higher stability, compared with known mesoMOFs and In(III)-based MOFs (Table S8). For such a stable mesoMOF, the activating method with boiling water can be highlighted to mostly demonstrate its mesoporous feature from gas adsorption isotherms. Remarkably, the stability is well recognized to be significant to the promising device applications for mesoMOFs, such as supercapacitor with higher specific capacitance and recycle capability, which may open up new opportunities for mesoMOFs materials as the platforms for clean energy sources.

Journal of Materials Chemistry A Accepted Manuscript

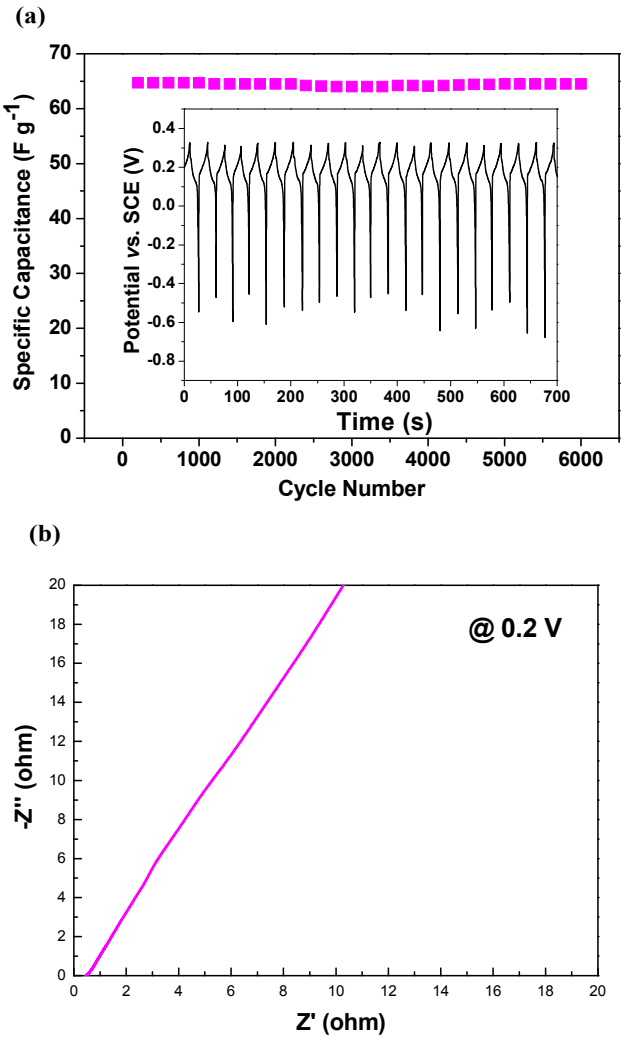

Fig. 6 (a) Charge/discharge cycling test of 437-MOF electrode at 4 A g^{-1} (inset: galvanostatic charge/discharge cyclic curves of the first and last 20 cycles). (b) Nyquist plot of 437-MOF electrode.

Acknowledgements

This work was financially supported by the National Natural Science Foundation of China (21031002, 91122005, 21171151, and 21201154), Plan for Scientific Innovation Talent of Henan Province, Program for Innovative Research Team in University of Tianjin (TD12-5038), and Program for New Century Excellent Talents in University of China (NCET-10-0143). We also thank Prof. D.-Q. Yuan (Fujian Institute of Research on the Structure of Matter) for helpful discussions on gas sorption.

Notes and references

[a] College of Chemistry, Tianjin Key Laboratory of Structure and Performance for Functional Molecules, MOE Key Laboratory of Inorganic-Organic Hybrid Functional Material Chemistry, Tianjin Normal University, Tianjin 300387, China. E-mail: dumiao@public.tpt.tj.cn

[b] Henan Provincial Key Lab of Surface & Interface Science, Zhengzhou University of Light Industry, Zhengzhou 450002, Henan, China. E-mail: chunsenliu@zzuli.edu.cn

† Electronic Supplementary Information (ESI) available: Further details for experiments, structural figures, schemes, and tables. CCDC 952936, 952937, and 952938. For ESI and crystallographic data in CIF or other electronic format see DOI: 10.1039/b000000x/

1 (*a*) G. Férey, *Chem. Soc. Rev.*, 2008, **37**, 191–214; (*b*) O. K. Farha and J. T. Hupp, *Acc. Chem. Res.*, 2010, **43**, 1166–1175; (*c*) K. K. Tanabe and S. M. Cohen, *Chem. Soc. Rev.*, 2011, **40**, 498–519; (*d*) H. Furukawa, K. E. Cordova, M. O'Keeffe and O. M. Yaghi, *Science*, 2013, **341**, 1230444; (*e*) M. Du, C.-P. Li, C.-S. Liu and S.-M. Fang, *Coord. Chem. Rev.*, 2013, **257**, 1282–1305.

2 (*a*) J.-R. Li, J. Sculley and H.-C. Zhou, *Chem. Rev.*, 2012, **112**, 869–932; (*b*) H. Wu, Q. Gong, D. H. Olson and J. Li, *Chem. Rev.*, 2012, **112**, 836–868; (*c*) P. Nugent, Y. Belmabkhout, S. D. Burd, A. J. Cairns, R. Luebke, K. Forrest, T. Pham, S. Ma, B. Space, L. Wojtas, M. Eddaoudi and M. J. Zaworotko, *Nature*, 2013, **495**, 80–84.

3 (*a*) L. Ma, C. Abney and W. Lin, *Chem. Soc. Rev.*, 2009, **38**, 1248–1256; (*b*) S. Bureekaew, S. Horike, M. Higuchi, M. Mizuno, T. Kawamura, D. Tanaka, N. Yanai and S. Kitagawa, *Nat. Mater.*, 2009, **8**, 831–836; (*c*) P. Horcajada, R. Gref, T. Baati, P. K. Allan, G. Maurin, P. Couvreur, G. Férey, R. E. Morris and C. Serre, *Chem. Rev.*, 2012, **112**, 1232–1268.

4 (*a*) Q.-R. Fang, T. A. Makal, M. D. Young and H.-C. Zhou, *Comments Inorg. Chem.*, 2010, **31**, 165–195; (*b*) W. Xuan, C. Zhu, Y. Liu and Y. Cui, *Chem. Soc. Rev.*, 2012, **41**, 1677–1695; (*c*) L. Song, J. Zhang, L. Sun, F. Xu, F. Li, H. Zhang, X. Si, C. Jiao, Z. Li, S. Liu, Y. Liu, H. Zhou, D. Sun, Y. Du, Z. Cao and Z. Gabelica, *Energy Environ. Sci.*, 2012, **5**, 7508–7520.

5 J. An, O. K. Farha, J. T. Hupp, E. Pohl, J. I. Yeh and N. L. Rosi, *Nat. Commun.*, 2012, **3**, 604.

6 D. Feng, Z.-Y. Gu, J.-R. Li, H.-L. Jiang, Z. Wei and H.-C. Zhou, *Angew. Chem. Int. Ed.*, 2012, **51**, 10307–10310.

7 (*a*) S.-T. Zheng, J. Bu, T. Wu, C. Chou, P. Feng and X. Bu, *Angew. Chem. Int. Ed.*, 2011, **50**, 8858–8862; (*b*) J. Reboul, S. Furukawa, N. Horike, M. Tsotsalas, K. Hirai, H. Uehara, M. Kondo, N. Louvain, O. Sakata and S. Kitagawa, *Nat. Mater.*, 2012, **11**, 717–723.

8 D.-Y. Hong, Y. K. Hwang, C. Serre, G. Férey and J.-S. Chang, *Adv. Funct. Mater.*, 2009, **19**, 1537–1552.

9 F. Gándara, B. Gomez-Lor, E. Gutiérrez-Puebla, M. Iglesias, M. A. Monge, D. M. Proserpio and N. Snejko, *Chem. Mater.*, 2008, **20**, 72–76.

10 M. Eddaoudi, J. Kim, N. Rosi, D. Vodak, J. Wachter, M. O'Keeffe and O. M. Yaghi, *Science*, **2002**, *295*, 469–472.

11 H. Deng, S. Grunder, K. E. Cordova, C. Valente, H. Furukawa, M. Hmadeh, F. Gándara, A. C. Whalley, Z. Liu, S. Asahina, H. Kazumori, M. O'Keeffe, O. Terasaki, J. F. Stoddart and O. M. Yaghi, *Science*, 2012, **336**, 1018–1023.

12 D. Zhao, D. J. Timmons, D. Yuan and H.-C. Zhou, *Acc. Chem. Res.*, 2011, **44**, 123–133.

13 N. L. Rosi, J. Kim, M. Eddaoudi, B. Chen, M. O'Keeffe and O. M. Yaghi, *J. Am. Chem. Soc.*, 2005, **127**, 1504–1518.

14 H. Li, M. Eddaoudi, M. O'Keeffe and O. M. Yaghi, *Nature*, 1999, **402**, 276–279.

Journal of Materials Chemistry A Accepted Manuscript

This journal is © The Royal Society of Chemistry 2014

15 J. J. Perry IV, J. A. Perman and M. J. Zaworotko, *Chem. Soc. Rev.*, 2009, **38**, 1400–1417.
16 A. L. Spek, *J. Appl. Crystallogr.*, 2003, **36**, 7–13.
17 Q.-R. Fang, G.-S. Zhu, Z. Jin, Y.-Y. Ji, J.-W. Ye, M. Xue, H. Yang, Y. Wang and S.-L. Qiu, *Angew. Chem. Int. Ed*., 2007, **46**, 6638–6642.
18 S.-H. Lo, C.-H. Chien, Y.-L. Lai, C.-C. Yang, J. J. Lee, D. S. Raja and C.-H. Lin, *J. Mater. Chem. A*, 2013, **1**, 324–329.
19 S. R. Batten, S. M. Neville and D. R. Turner, *Coordination polymers: Design*, *analysis and application*, RSC Publishing, Cambridge, 2008.
20 K. A. Cychosz and A. J. Matzger, *Langmuir*, 2010, **26**, 17198–17202.
21 K. S. Walton and R. Q. Snurr, *J. Am. Chem. Soc.*, 2007, **129**, 8552–8556.
22 Y. K. Park, S. B. Choi, H. Kim, K. Kim, B.-H. Won, K. Choi, J.-S. Choi, W.-S. Ahn, N. Won, S. Kim, D. H. Jung, S.-H. Choi, G.-H. Kim, S.-S. Cha, Y. H. Jhon, J. K. Yang and J. Kim, *Angew. Chem. Int. Ed.*, 2007, **46**, 8230–8233.
23 Y.-B. Zhang, W.-X. Zhang, F.-Y. Feng, J.-P. Zhang and X.-M. Chen, *Angew. Chem. Int. Ed.*, 2009, **48**, 5287–5290.
24 S. J. Gregg and K. S. W. Sing, *Adsorption, surface area and porosity*, Academic Press, London, 1982.
25 K. S. Walton, A. R. Millward, D. Dubbeldam, H. Frost, J. J. Low, O. M. Yaghi and R. Q. Snurr, *J. Am. Chem. Soc.*, 2008, **130**, 406–407.
26 S. Yang, X. Lin, W. Lewis, M. Suyetin, E. Bichoutskaia, J. E. Parker, C. C. Tang, D. R. Allan, P. J. Rizkallah, P. Hubberstey, N. R. K. Champness, M. Thomas, A. J. Blake and M. Schröder, *Nat. Mater.*, 2012, **11**, 710–716.
27 (*a*) P. Simon and Y. Gogotsi, *Nat. Mater.*, 2008, **7**, 845–854; (*b*) S.-L. Li and Q. Xu, *Energy Environ. Sci*., 2013, **6**, 1656–1683.
28 (*a*) H. Wang, H. S. Casalongue, Y. Liang and H. Dai, *J. Am. Chem. Soc.*, 2010, **132**, 7472–7477; (*b*) V. Dusastre, *Materials for Sustainable Energy*, Macmillan Publishers Ltd., 2011; (*c*) Q. Lu, M. W. Lattanzi, Y. Chen, X. Kou, W. Li, X. Fan, K. M. Unruh, J. G. Chen and J. Q. Xiao, *Angew. Chem. Int. Ed.*, 2011, **50**, 6847–6850; (*d*) Z. Tang, C.-H. Tang and H. Gong, *Adv. Funct. Mater.*, 2012, **22**, 1272–1278.
29 K. R. Prasad, K. Koga and N. Miura, *Chem. Mater.*, 2004, **16**, 1845–1847.
30 M. Toupin, T. Brousse and D. Bélanger, *Chem. Mater.*, 2002, **14**, 3946–3952.
31 S. K. Meher, P. Justin and G. R. Rao, *ACS Appl. Mater. Interfaces*, 2011, **3**, 2063–2073.
32 L.-Q. Mai, F. Yang, Y.-L. Zhao, X. Xu, L. Xu and Y.-Z. Luo, *Nat. Commun.*, 2011, **2**, 381.
33 M. Winter and R. J. Brodd, *Chem. Rev.*, 2004, **104**, 4245–4269.
34 X. Lang, A. Hirata, T. Fujita and M. Chen, *Nat. Nanotech.*, 2011, **6**, 232–236.
35 (*a*) S. C. Canobre, D. A. L. Almeida, C. P. Fonseca and S. Neves, *Electrochim. Acta*, 2009, **54**, 6383–6388; (*b*) S. K. Meher and G. R. Rao, *J. Phys. Chem. C*, 2011, **115**, 15646–15654.
36 (*a*) W. Xiao, H. Xia, J.-Y.-H. Fuh and L. Lu, *J. Electrochem. Soc.*, 2009, **156**, A627–A633; (*b*) R. B. Rakhi, W. Chen, D. Cha and H. N. Alshareef, *Adv. Energy Mater.*, 2012, **2**, 381–389.

Journal of Materials Chemistry A Accepted Manuscript

Graphical Abstract

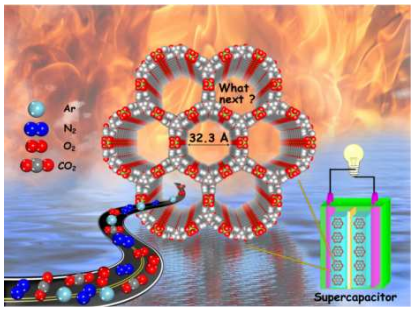

A mesoporous metal–organic framework with perfect 1-D hexagonal channels and high physicochemical stability represents a promisiding candidate for electrode material of supercapacitor.

Journal of Materials Chemistry A Accepted Manuscript